Published in the USA
European Geographical Studies
Issued since 2013.
E-ISSN: 2413-7197
2025. 12(1): 9-25

DOI: 10.13187/egs.2025.1.9
https://egs.cherkasgu.press

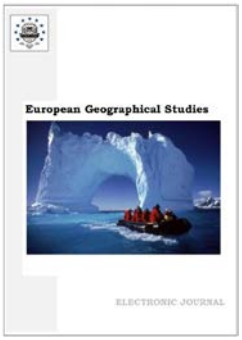

Technical Notes on the Applicability of SEM And EPMA (Microprobe Analysis) for Reconstructing Biogeographical and Paleoclimatic Factors of Taphonomic Alterations of Elasmobranch Teeth

Pavel L. Alexandrov [a, b, *], Mikhail K. Filippov [c], Theodor K. Orekhov [c]

[a] Institute of Higher Nervous Activity and Neurophysiology, RAS, Moscow, Russian Federation
[b] Shemyakin-Ovchinnikov Institute of Bioorganic Chemistry, RAS, Moscow, Russian Federation
[c] Semenov Institute of Chemical Physics, RAS (ICP RAS), Moscow, Russian Federation

Abstract

Fossil elasmobranch teeth collected from multiple geographic regions, contrasting depositional settings, and different palaeo-oceans/palaeoclimates offer valuable archives of past marine conditions, but they pose a general analytical challenge for us: ensuring comparability among samples affected by locality-specific diagenesis. Primary biological and environmental signatures in enameloid and dentine can be partially overprinted by recrystallisation, mineral replacement, and post-burial elemental uptake. To discriminate these signals reliably, an integrated microstructural–geochemical workflow is required in which scanning electron microscopy is combined with electron-probe microanalysis with energy-dispersive (EDS) and wavelength-dispersive (WDS) X-ray spectroscopy. Deposits formed in different basins, palaeo-continents and palaeo-oceans commonly experienced contrasting diagenetic histories (chemistry, burial temperature, sedimentation time and substitution, redox state of the environment). These factors can overprint tooth tissues in ways that mimic or obscure primary biological/environmental signals. SEM provides the necessary taphonomic and microstructural context prior to geochemical interpretation. Backscattered-electron imaging and high-resolution secondary-electron imaging allow direct assessment of sample preservation states. SEM also resolves diagnostic enameloid ultrastructure, enabling the distinction between preserved biogenic fabrics and diagenetic mosaics that may mimic original biogenic features.

Keywords: biogeography, taphonomy, elasmobranchs, diagenesis, biomineralization, enameloid, SEM, EPMA, WDS, EDS, backscattered electron detector (BSE).

1. Introduction

A fundamental feature that underpins biogeographers' interest in studying fossil shark (elasmobranch) teeth is their ubiquitous occurrence across highly spatially separated regions, countries, and different continents, in particular:

1. In Australia and New Zealand (Daymond, 1999; Rees et al., 2024), as well as on the islands of the Malay Archipelago (e.g., Borneo), known in Western literature as Insulindia or the Indo-Australian Archipelago (Kocsis, 2024);

2. In Asia, specifically in:

* Corresponding author
E-mail addresses: geochemicalphysics@gmail.com (P.L. Alexandrov)

2.1. India (Prasad et al., 2004; Prasad et al., 2017).
2.2. Taiwan (Lin et al., 2022).
2.3. Thailand (Cappetta et al., 2006).
2.4. South Korea (Yun, 2021).
3. In Africa, both in North Africa (Adnet et al., 1990; Boulemia, Adnet, 2023) and in Southern Africa (Smale, 2005).
4. In Antarctica and adjacent islands (such as Seymour Island, also known as Simur, located near the Trinity Peninsula, the northern tip of the Antarctic Peninsula (Long, 1992)).
5. In Europe (Leidner, Thies, 1999), specifically in:
5.1. Austria (Feichtinger et al., 2025).
5.2. Belgium (Iserbyt, De Schutter, 2012).
5.3. The United Kingdom (Paton, 1993).
5.4. Germany (Höltke et al., 2023).
5.5. Western Kazakhstan (it is well known that most of the country's territory belongs to Central Asia, but some parts, including West Kazakhstan Region, lie in Europe, making Kazakhstan a transcontinental state) (Radwański, Marcinowski, 1996).
5.6. Poland (Schultz, 1977).
5.7. The European part of Russia (Mertiniene, 1995).
5.8. Ukraine (Sokolskyi, Guinot, 2021).
6. In North America, specifically in:
6.1. Canada (Beavan, Russell, 1999; Mutter et al, 2007).
6.2. The United States (Schubert, 2013; Shimada et al., 2015; Swinehart et al., 2020).
7. In South America/Latin America, specifically in:
7.1. Argentina (Johns et al, 2014).
7.2. Peru (Landini et al., 2017).
7.3. Chile (Suaez et al., 2004).

The study of fossil elasmobranch teeth requires analytical methods capable of resolving the hierarchical microstructure of enameloid and dentine, and quantifying chemical compositions at spatial scales comparable to growth tissues and diagenetic alteration fronts. Scanning electron microscopy (SEM) combined with electron-probe microanalysis (EPMA) with X‑ray microanalysis by wavelength-dispersive (WDS) or energy-dispersive spectroscopy (EDS) provides precisely this pairing of microstructural and microchemical evidence. This integrated approach is particularly necessary because fossil shark teeth are commonly preserved in markedly different biogeoghraphic and taphonomic states, and because enameloid exhibits tissue-specific crystal architectures that can be obscured or mimicked or disrupted by diagenesis and carious (chemo)taphonomic conditions.

2. Materials and methods.

2.1. Why SEM is necessary.

Elasmobranch tooth enameloid is a highly mineralised, apatite-based tissue whose diagnostic characters reside in micro- to nanoscale organisation: crystallite size and habit, preferred orientation, bundled architectures, and the nature of the enameloid–dentine junction (EDJ). Optical microscopy alone is often insufficient because many of these features are below the diffraction limit, and (sic!) diagenetic overprinting frequently modifies optical properties without preserving original textures.

Different SEM regimes are therefore used to:

1. Characterise enameloid ultrastructure. Secondary-electron imaging can reveal surface relief, permitting discrimination between primary crystallite bundles/orientation patterns and secondary recrystallised mosaics.
2. Identify diagenetic microtextures. Backscattered-electron (BSE) imaging provides compositional contrast (mean atomic number contrast), enabling recognition of infillings, coatings, and replacement phases (e.g., carbonate cement, silica, iron–manganese oxides) that may not be apparent in transmitted light.
3. Map microcracks, porosity, and intergranular boundaries. These are critical because they act as pathways for fluid-mediated element exchange and thus govern the spatial pattern of chemical alteration.

4. SEM allows analysts to select minimally altered regions of enameloid and dentine and target specific structural units (enameloid vs dentine).

SEM provides the microstructural context required to interpret any chemical data as either biogenic (primary) or diagenetic (secondary).

2.2. Why EPMA is necessary

EPMA (electron microprobe) offers quantitative, spatially resolved major- and minor-element analysis at the micrometre scale, which matches the scale of tooth tissues and many alteration halos. This is essential because elasmobranch teeth comprise compositionally distinct components (enameloid vs dentine), and diagenesis can create steep chemical gradients over tens of micrometres. EPMA is used to:

1. Quantify apatite stoichiometry and substitutions. Measuring Ca, P, and minor elements (e.g., F, Na, Mg, S, Cl, Sr) constrains the degree and type of ionic substitution in bioapatite, which in turn reflects both original biomineralisation and diagenetic modification (e.g., fluoridation, carbonate substitution proxies, coupled substitutions).

2. Distinguish tissue-specific signatures. Enameloid and dentine often differ in minor-element budgets and alteration susceptibility; quantitative traverses can reveal whether chemical contrasts are primary or have been homogenised by recrystallisation.

3. Resolve microchemical heterogeneity. Preservation is rarely uniform; EPMA maps and line scans can identify diffusion fronts, secondary mineral microdomains, and compositional zonation associated with cracks or pore spaces.

4. Provide robust comparability across specimens of differing preservation. Quantitative microprobe data permit objective comparison when macroscopic appearance is misleading.

2.3. Why both WDS and EDS are needed

Although both WDS and EDS detect characteristic X‑rays generated under the electron beam, they differ in spectral resolution, sensitivity, and analytical reliability. Fossil teeth frequently contain complex, mixed-phase assemblages (apatite plus diagenetic precipitates), making spectral interferences and low-level substitutions a routine problem. Employing both techniques is therefore scientifically justified. EDS (energy-dispersive spectroscopy) is used to:

a) Rapidly screen phases and heterogeneities. EDS is well suited for reconnaissance mapping to locate diagenetic phases (e.g., Fe-rich coatings, Mn oxides, silica infill, carbonate cement) and to prioritise domains for quantitative work.

b) Provide broad-area compositional maps quickly. This is valuable for documenting preservation variability within a single tooth, and for identifying “least altered” regions for subsequent WDS/EPMA.

However, EDS has limitations relevant to enameloid studies: lower energy resolution increases the risk of peak overlaps; detection limits are typically poorer for trace-to-minor elements; and quantification of light elements (notably F, Na, Mg) can be less reliable in complex matrices. WDS (wavelength-dispersive spectroscopy) is used to:

a) Obtain high-precision, interference-resolved quantification. WDS provides superior spectral resolution, reducing misidentification and improving accuracy where peak overlaps matter.

b) Measure minor and light elements critical to apatite chemistry. In fossil enameloid, elements such as F, Na, Mg, S, and Cl can be pivotal for distinguishing primary mineralisation from diagenetic fluoridation or contamination; WDS typically delivers the precision and lower detection limits needed for these interpretations.

c) Support defensible comparisons among differently preserved specimens. Because WDS is more robust for subtle compositional differences, it is preferable for testing hypotheses about diagenetic overprint versus retained biogenic signals.

Thus, EDS is most effective for efficient phase recognition and spatial reconnaissance, whereas WDS is essential for rigorous, publication-grade quantification of key elements in apatite and associated alteration products.

2.4. Biogeographical aspects of SEM visualization and EPMA/WDS/EDS analysis of elasmobranch teeth.

When fossil shark teeth are collected from different geographic regions, deposits with contrasting geochemical regimes, different continents, and different palaeo-oceans and

palaeoclimates, the main scientific challenge is comparability: you must separate (i) original biological and environmental signals recorded in enameloid/dentine from (ii) locality-specific diagenetic overprint (replacement, recrystallisation, elemental uptake). The combined use of SEM, EPMA, WDS and EDS is justified because it links microstructure to chemistry at the same spatial scale where both primary growth features and diagenetic alteration occur.

EPMA or SEM with WDS and/or EDS provides the microstructural and taphonomic "context" needed before any geochemical interpretation can be trusted.

a) Assess preservation and diagenesis directly: SEM imaging (especially BSE) reveals recrystallisation textures, secondary cements/infillings, microcracks, and porosity networks that control fluid access. These features vary strongly between deposits and between palaeoceanographic regimes.

b) Resolve enameloid ultrastructure: Shark enameloid has diagnostic crystallite structures (orientation, bundles, layering) that can be partially destroyed or mimicked by diagenetic mosaics. SEM with WDS and/or EDS can distinguish preserved ultrastructure from replacement textures and their chemical mapping.

c) Define where to analyse: Because alteration is often patchy within a single tooth, SEM is essential for selecting minimally altered enameloid/dentine domains and avoiding contaminated margins or crack-hosted precipitates. Without microanalysis (such as EPMA), chemical differences could simply reflect unequal preservation, not real palaeoenvironmental variation. EPMA provides quantitative, micrometre-scale element concentrations, which is the appropriate scale for tooth tissues and alteration fronts.

d) Quantify apatite chemistry and substitutions: Measuring Ca and P plus minor elements (e.g., F, Na, Mg, S, Cl, Sr) helps determine whether the tissue remains close to biogenic apatite or has been chemically transformed (e.g., ion exchange which can be correlated with different geochemical and paleogeographical conditions). EPMA therefore underpins any attempt to compare fossils from different basins, continents, and palaeoclimatic zones.

EDS (energy-dispersive X-ray spectroscopy) advantages are:

– Fast phase identification and screening: Quickly shows where Fe/Mn-rich coatings, silica infillings, carbonate cements, or clay contamination occur—features that can differ systematically between deposits and continents.

– Rapid compositional mapping: Useful for documenting heterogeneity across many specimens/localities and for choosing targets for precise analyses.

WDS (wavelength-dispersive X-ray spectroscopy) advantages are:

– Higher spectral resolution and fewer peak-overlap problems: Critical in apatite-rich materials where interferences can bias results, especially when comparing subtle differences between regions.

– Better precision and lower detection limits for key minor/light elements: Elements such as F, Na, Mg, S and Cl are central for diagnosing diagenetic alteration versus primary signals; WDS is typically required for defensible measurements.

– Stronger basis for inter-site comparisons: When interpreting differences between palaeo-oceans/palaeoclimates, you often expect small but meaningful shifts in composition; WDS provides the analytical confidence to test those hypotheses.

Why this complex integrated approach is essential for multi-continent, multi-basin palaeoenvironmental interpretation? Different deposits and palaeo-oceans impose different diagenetic pathways (fluid chemistry, temperature, burial history, redox conditions), which can overprint teeth in different ways. The combined SEM–EPMA–EDS/WDS workflow allows you to:

a) Distinguish primary (biogenic/environmental) signals from secondary (diagenetic) signals by tying chemistry to microtextures and alteration pathways.

b) Identify and exclude altered domains so comparisons between continents are not driven by uneven preservation.

c) Document deposit-specific diagenetic signatures (e.g., crack-hosted Fe–Mn enrichments, fluoridation halos, cement infiltration), preventing false palaeoclimatic or palaeoceanographic conclusions.

d) Produce reproducible, standardised datasets suitable for large-scale geographic and stratigraphic comparisons.

2.5. Old SEM automation

2.5.1. Reprogramming of the SEM Registration System Based on DIGIC III Processor.

For SEM image and video registration a DIY system was adapted with a Canon A590IS CCD sensor (maximum resolution 3264 x 2448 pixels in static mode; maximum video recording resolution 640x480 with a maximum video frame rate of 30 frames per second when using the MJPEG video codec) and a Canon DIGIC III image processor, synchronized directly from the control system of the electron microscope through a special cable based on a universal bus cable. The registration system was mounted on a 3D-printed module, compatible in size with the Canon A590IS mount. The key requirement for the image registration system implemented on the DIGIC processor was supporting of CHDK - a resident program that expands the control functions of Canon digital cameras. CHDK program was installed to the SD card as follows:

1. On a PC with pre-installed JAVA, the installer of CHDK ("STICK") was unpacked and one of its files – either STICK.BAT or STICK.CMD was started (one of them may not provide a successful CHDK installation).
2. Testing was performed using a random SEM image.
3. After completion, the flag on the memory card was transferred to the "Lock" position.
4. Using the camera buttons <Print> and <Menu> CHDK menu was entered.
5. Pressing <Set> allowed to enter the <Enhanced photo operations> section.
6. Using the <Set>, <Up> and <Down> buttons, the following camera parameters were set:

a. Disable overrides – No

b. Override TV type – long exp

c. Long exp value – the exposure required by the SEM (in the case of Jeol JSM-T330A it is 38 seconds for scanning)

d. Override AV, Override ISO, Subj dist – the following values for aperture, ISO and focal length were applied: 20, 12 and 250. After setting the numerical values of the above parameters, checkboxes should appear to the left of the values, confirming the values entered

e. Disable overrides on start – the corresponding checkmark should be removed, since this option makes CHDK save the values entered after the camera is turned off.

7. Double clicking <Menu> returns to the main menu, and then using <Set>, <Up>, <Down> find "CHDK settings" section, "Remote parameters" subsection.
8. "Enable remote", "Switch type – one push", "Control mode – normal" parameters were set.

2.5.2. Synchronization Line Upgrade.

A new synchronization line was developed to control the photoregistration procedure. To synchronize with SEM, pulses with a voltage of 3-5 V and a current of up to 10 milliamperes were used, supplied through the power lines of the USB input of the camera with the standard polarity. The appearance of the signal is equivalent to a partial pressing the photographing button, and the disappearance of the signal is equivalent to pressing the button completely (i.e., starting the photographing). When creating a synchronization line between Jeol JSM-T330A and Canon A590IS using a USB-A - mini-USB-B cable, the following operations were performed:

1. USB-A connector was cut off, after which it was required to free, strip and tin the black and red wires (color marking is standard for the universal serial bus), the white and green wires can be cut off.

2. The cap on the right side of the front panel of the electron microscope was removed and the screws for fixing the strip with the <Shutter> button were unscrewed.

3. The ground and power lines were found on the board nearest to the <Shutter> button using easily detectable designations on the pinout of any microcircuit: ground is designated as Gnd, power as Vcc. The <Shutter> button has two switch contact groups, one of which is not used. To the latter unused normally open pair of contacts the red wire of the USB cable and the power line found in accordance with the above instructions were soldered.

4. The black wire was soldered to the ground line.

5. The criterion for correctness during testing of the system was that when the cable was connected to the camera and the <Shutter> button was pressed, shooting automatically starts.

The advantages of Canon A590IS include the ability to simultaneously connect a USB cable, a power supply and an analog video signal transduction cable. Therefore, we also implemented an

image output to the analog monitor from the analog signal transmission cable. It is also possible to use a camera that does not have an additional power input and video output, but it is less convenient.

2.5.3. Creating an Adapter for Optical Registration Tract from the SEM CRT.

A special adapter was created for optical connection of the camera to the microscope screen. Its parameters depend on the system used. For the case of the Jeol JSM-T330A – Canon A590IS system, the following model was used: https://www.tinkercad.com/things/2i7MgsxqgKt-sem (Figure 1). The model was printed on a standard type 3D printer with black PLA filament FDplast. There are no specific requirements for the surface treatment of such products. However, when preparing a 3D model for printing, it is necessary to make sure that no supports are added inside the side tube. The rest of the settings are standard.

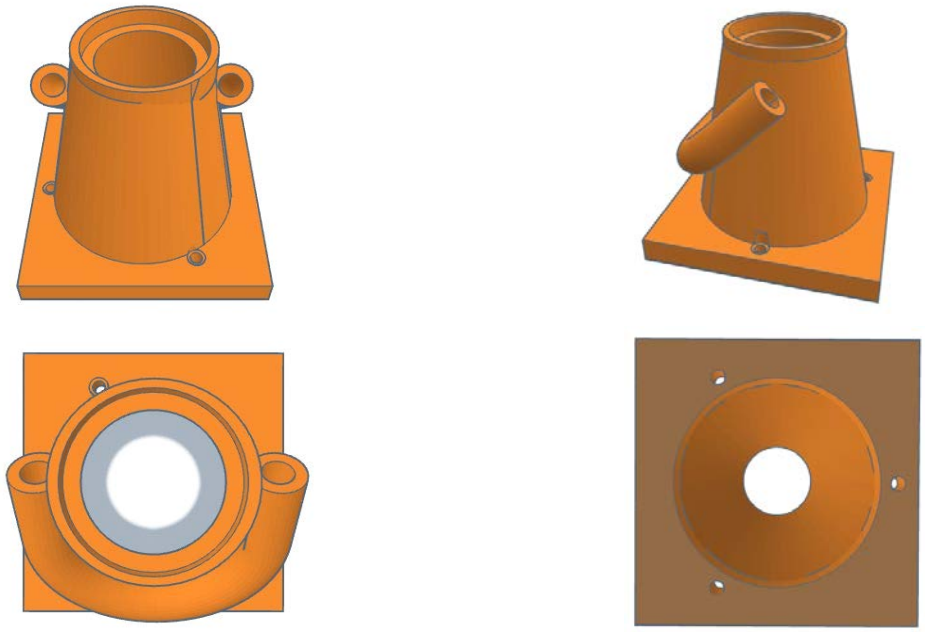

Fig. 1. 3D printable adapter for optical registration tract from the CRT of the JEOL SEM

The adapter is attached to the film camera mounting system of the microscope, and the Canon A590IS is attached using a cable tie that goes through the side tube (Figure 2).

Fig. 2. Canon A590IS fixation on the 3D printable adapter for optical registration tract from the CRT

2.5.4. Power Supply Optimization.

A power supply unit (3 V, plus in the center) was connected to the registration system, allowing it to operate without using batteries or accumulators. In this case, automatic shutdown was disabled in the camera settings, and the screen was turned off in the CHDK settings (<Print> -> <Menu> -> “CHDK settings”, then “Disable LCD off” is selected and using the <Set> button is switched to the "always on" mode).

2.5.5. Output To An External Liquid Crystal Or Plasma Monitor.

It is also possible to improve the view of the small screen of the microscope by connecting to the camera a TV with analog video input via AVC-BC300 or STV-250N cable or a standard camcorder cable (see the scheme below) or the Scart input (via the same cable and Video-Scart adapter). The above scheme is shown in details in Fig. 3, and the resulting view of the system after upgrade is shown in Figure 4.

Canon SX150IS (STV-250N cable)

	1	2	3	4
Archos, Gigabeat, Creative Zen Vision Series, Cown iAudio, Apple iBook	Ground	Video	Right	Left
Standard Camcorder Cable	Right	Ground	Video	Left
iPod Video	Video	Ground	Left	Right
Zune	Video	Ground	Right	Left

Fig. 3. Contact scheme for the Canon A590IS

Fig. 4. General view of the installation after upgrade

a

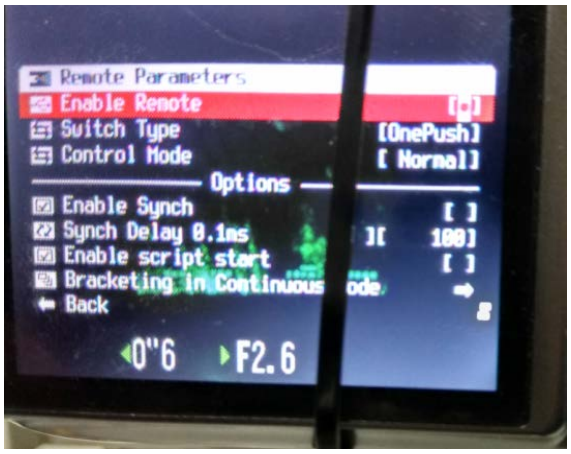

b

Fig. 5. Installation configuring on the Canon A590IS panel for the SEM image registration

2.5.6. Photography Process After Upgrade.

a) The following procedures are required to obtain digital SEM images from Jeol JSM-T330A:

1. Adjustment of the image parameters is carried out as usual using the knobs and buttons on the electron microscope control panel.
2. The minimum Spot size is set, brightness and contrast are matched.
3. The exposure time of frames is adjusted (in the case of Jeol JSM-T330A press the “Qucik” key located to the left of the “Shutter” button).
4. The photocamera cover is closed.
5. The camera turns on. In the case of Canon A590IS, the camera should be in “M” (manual) mode and manual focus should be selected (approximately 20-25).
6. For Jeol JSM-T330A, it is necessary to achieve blanking of the screen persistence. For this, the "Slow 1" key is dropped first; without releasing it, one needs to wait 3-4 seconds; after that the “Shutter” key is lowered, the “Slow 1” key is released, then the “Shutter” key is also released (Figure 5).
7. If everything has been done correctly, the camera takes a frame from the microscope screen during the exposure time, then during the same time it takes a dark frame, subtracts the latter fro the former, and saves it at the SD card.
8. The images obtained can be conveniently processed by IrfanView softwave in the following algorithm: “File → Batch conversion/rename → Advanced”. In particular, monochromatization, cropping, contrasting (if necessary) can be carried out through this algorithm in batch processing of the entire image series stereotypically (Figure 6).

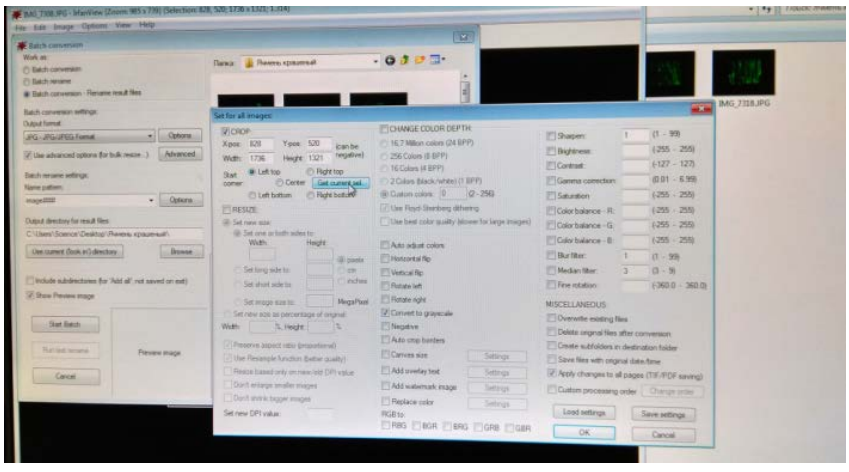

a

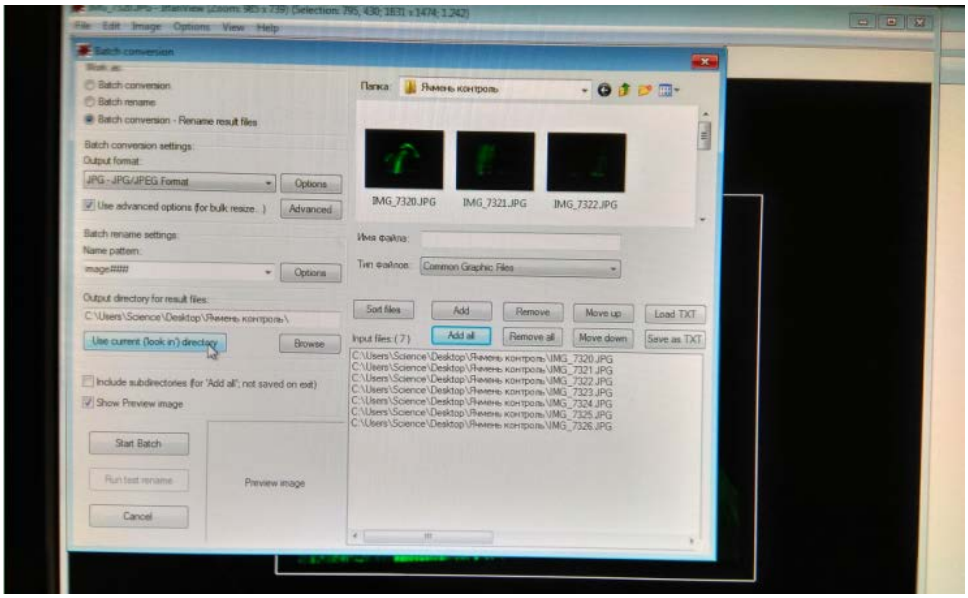

b

Fig. 6. Basic SEM image processing configuration for IrfanView softwave

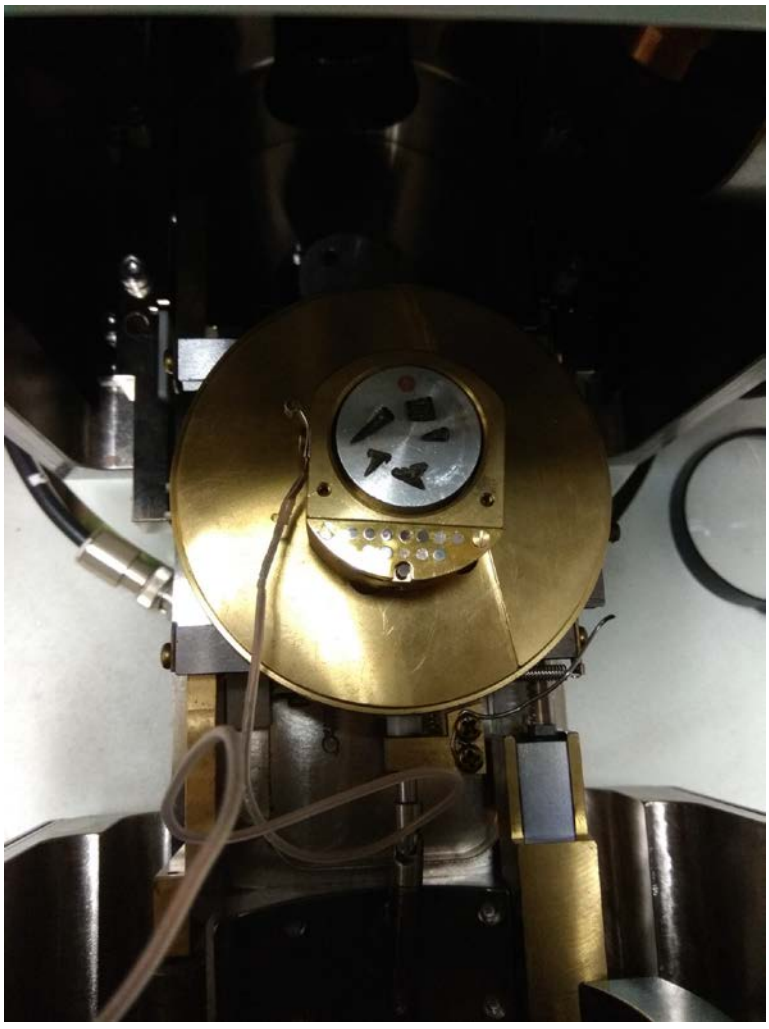

a

Fig. 7. Elasmobranch tooth samples on the rotating SEM stage (standpoint A)

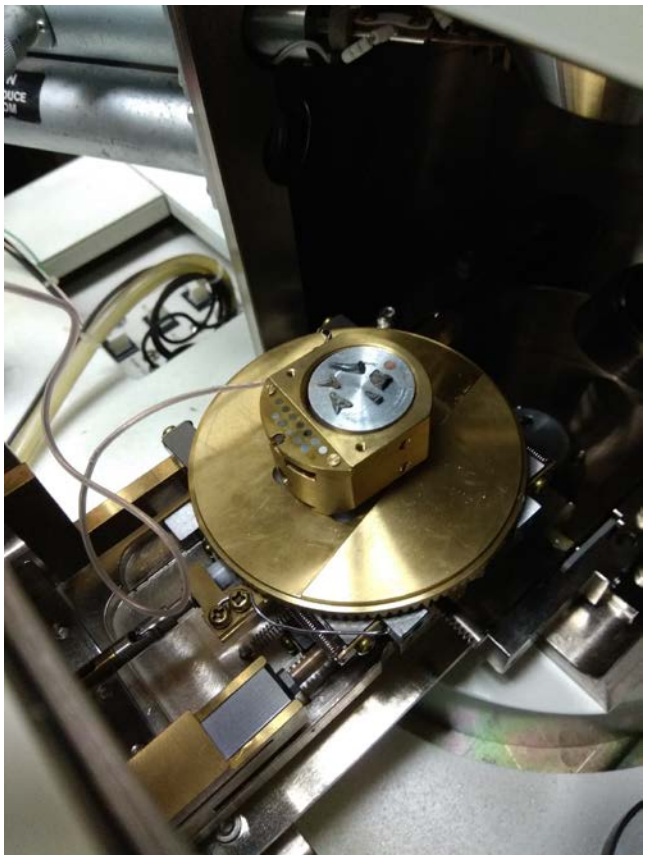

b

Fig. 7. Elasmobranch tooth samples on the rotating SEM stage (standpoint B).

3. Results

Results – SEM micrograph images of fossilized elasmobranchs/fossil shark teeth at different magnifications in the image series below (for small teeth which can be analyzed on the rotating stage of the SEM – see Figure 7a, Figure 7b – and on the Rowland circle):

Figure 8. General view of the tooth at 35x, scale bar – 500 µm. Acceleration voltage – 5 kV. Figure 8a shows the micrograph of the final product; Figure 8b shows its colorization using artificial intelligence.

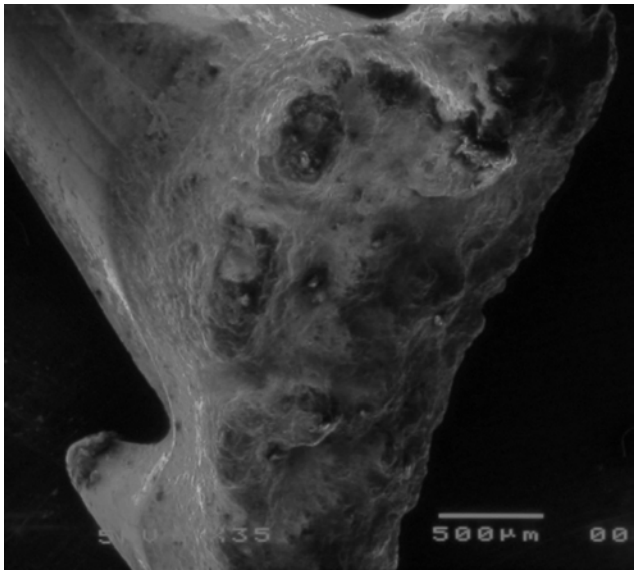

a

b

Fig. 8. General view of the tooth at 35x magnification (a – original micrograph; b – its colorization using artificial intelligence), scale bar/scale bar – 500 µm. Acceleration voltage – 5 kV

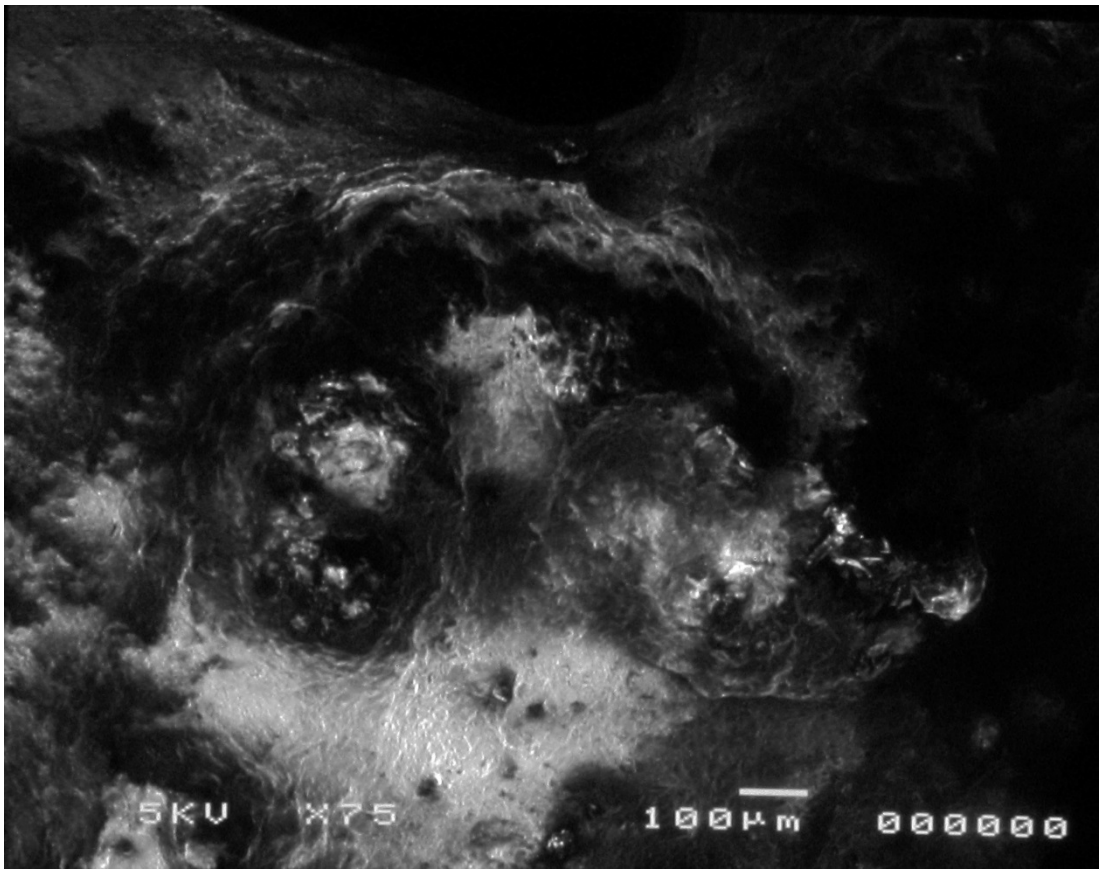

Fig. 9. The same sample. Magnification 75x, scalebar 100 µm, accelerating voltage 5 kV

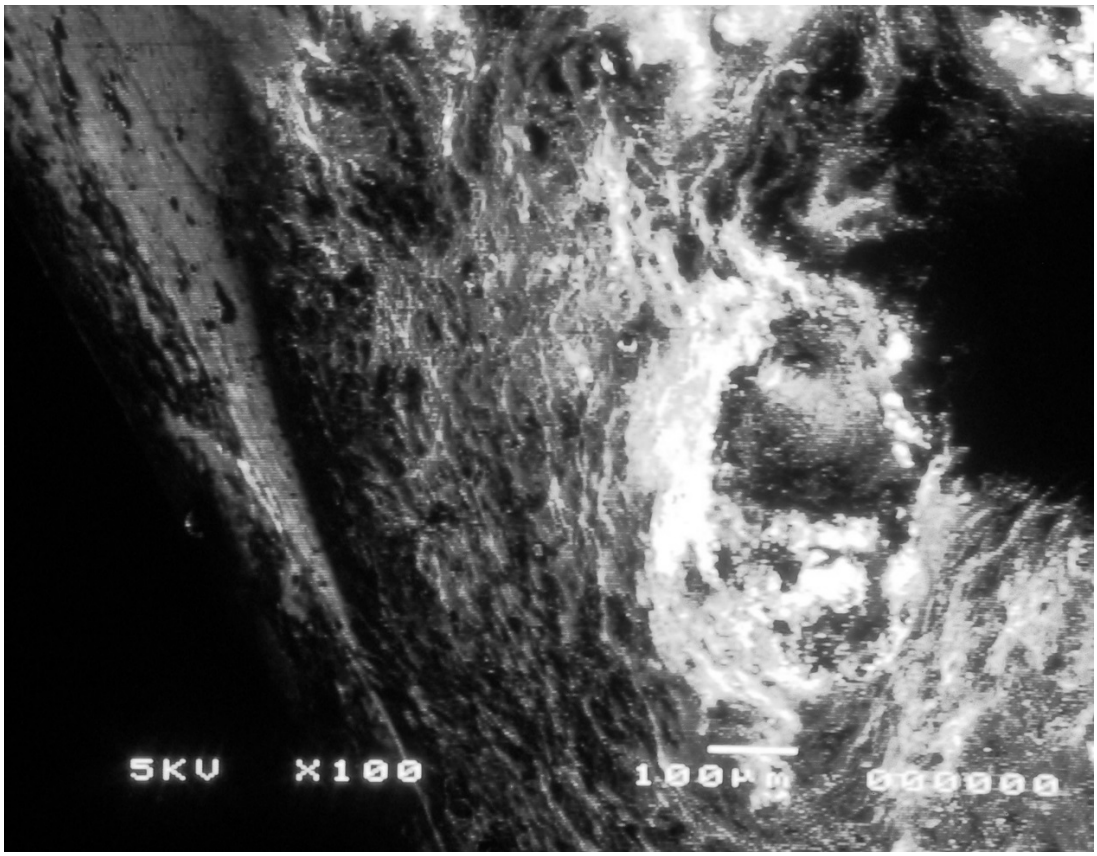

Fig. 10. The same sample. Magnification 100x, scalebar 100 μm, accelerating voltage 5 kV

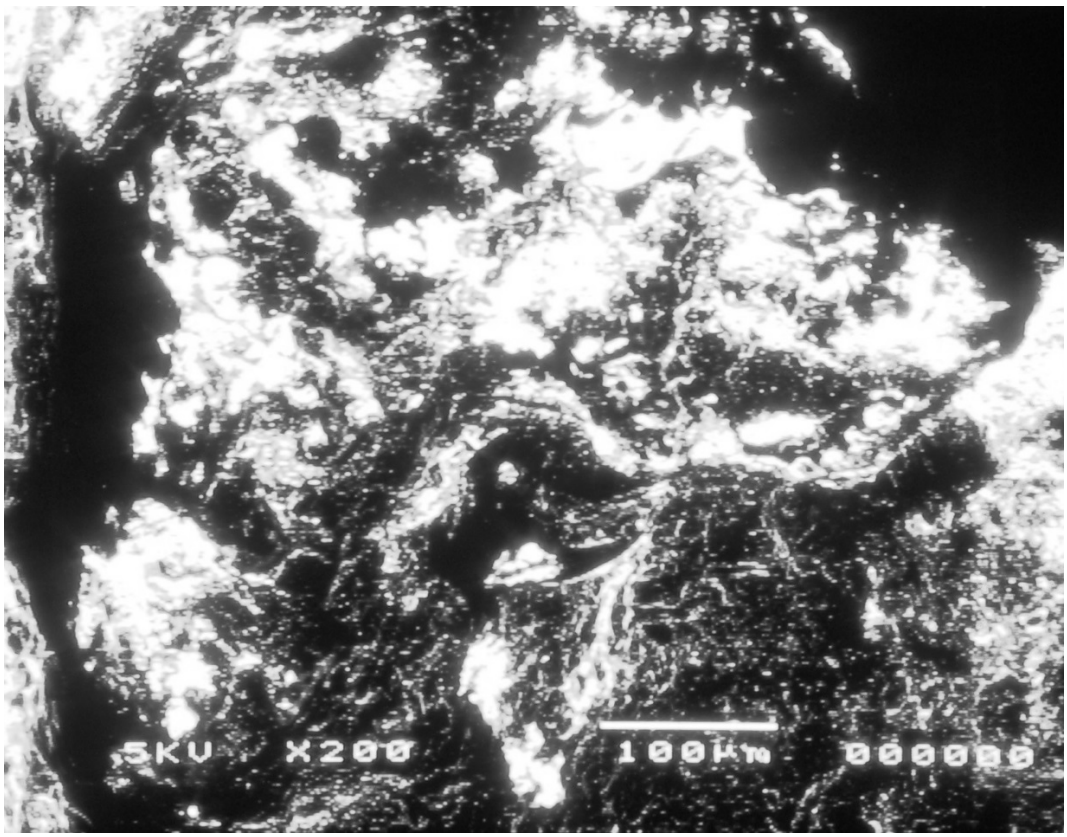

Fig. 11. The same sample. Magnification 200x, scalebar 100 μm, accelerating voltage 5 kV

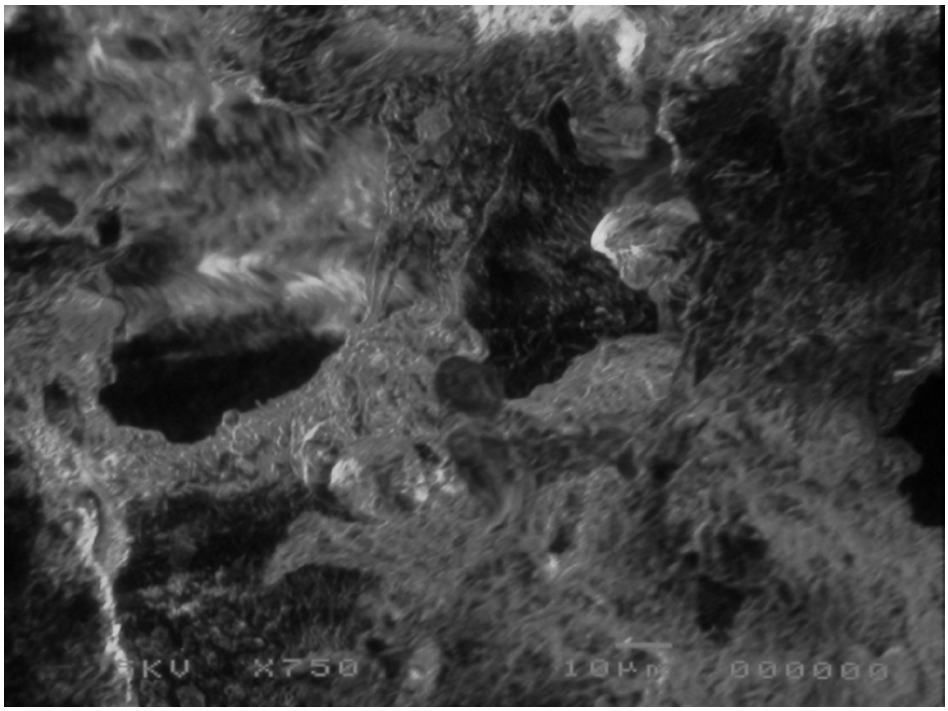

Fig. 12. The same sample. Magnification 750x, scalebar 10 µm, accelerating voltage 5 kV

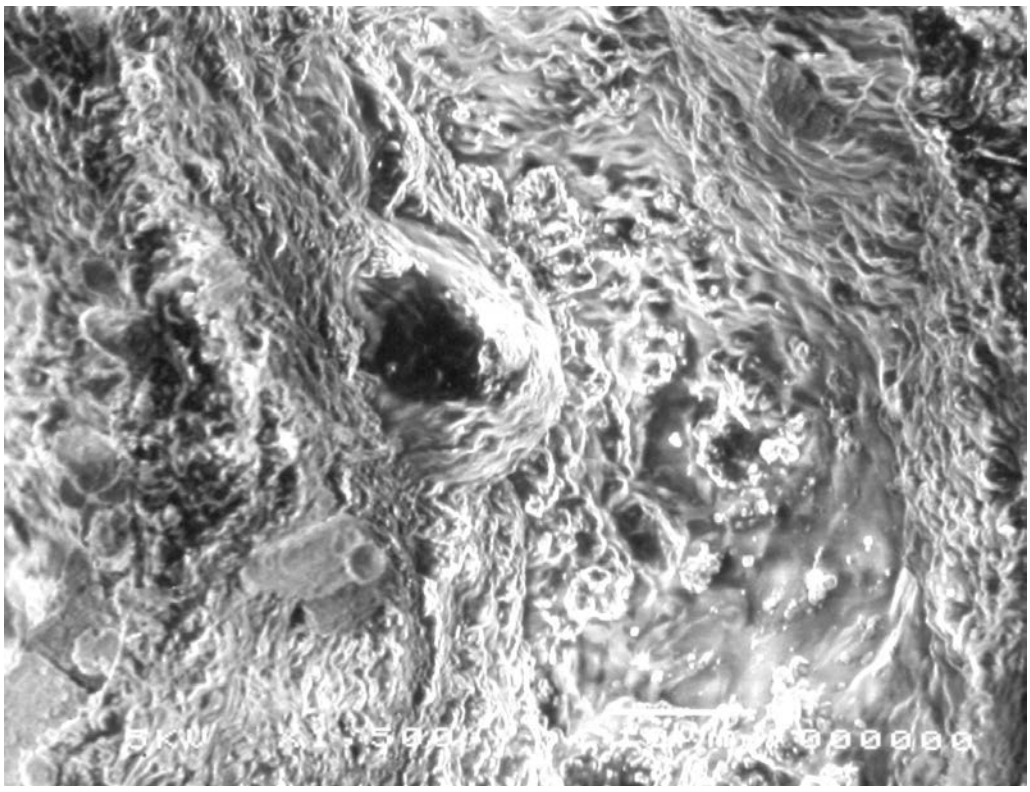

Fig. 13. The same sample. Magnification 1500x, scalebar 10 µm, accelerating voltage 5 kV

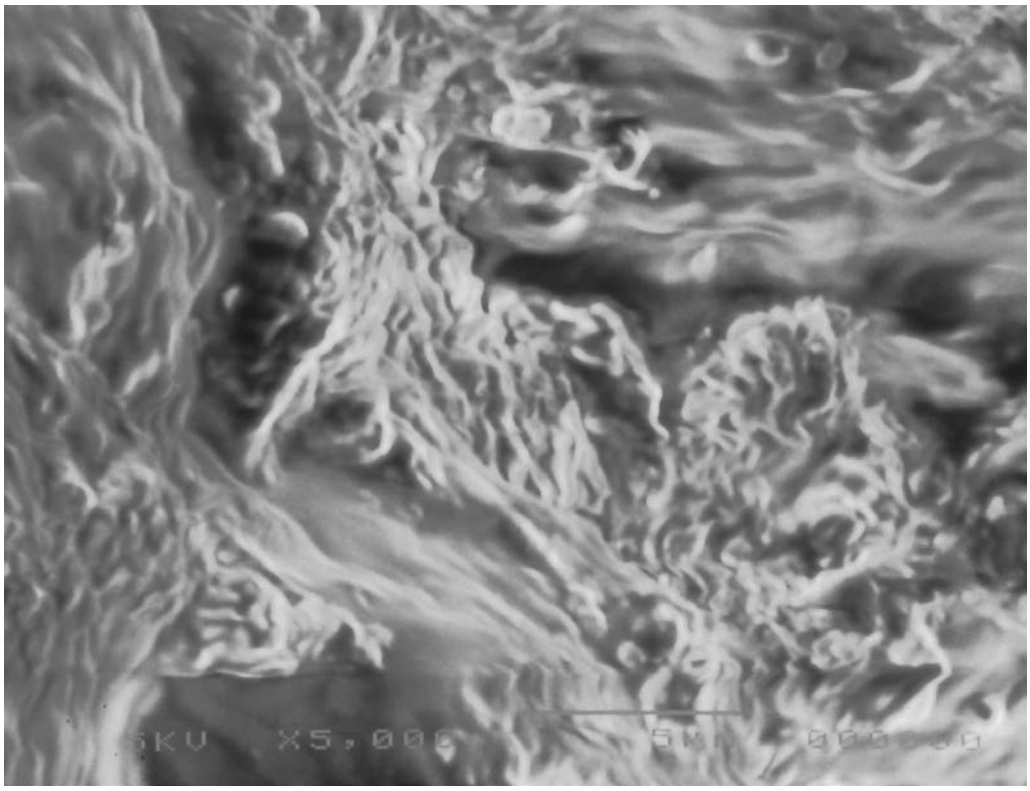

Fig. 14a. The same sample. Magnification 5000x, accelerating voltage 5 kV

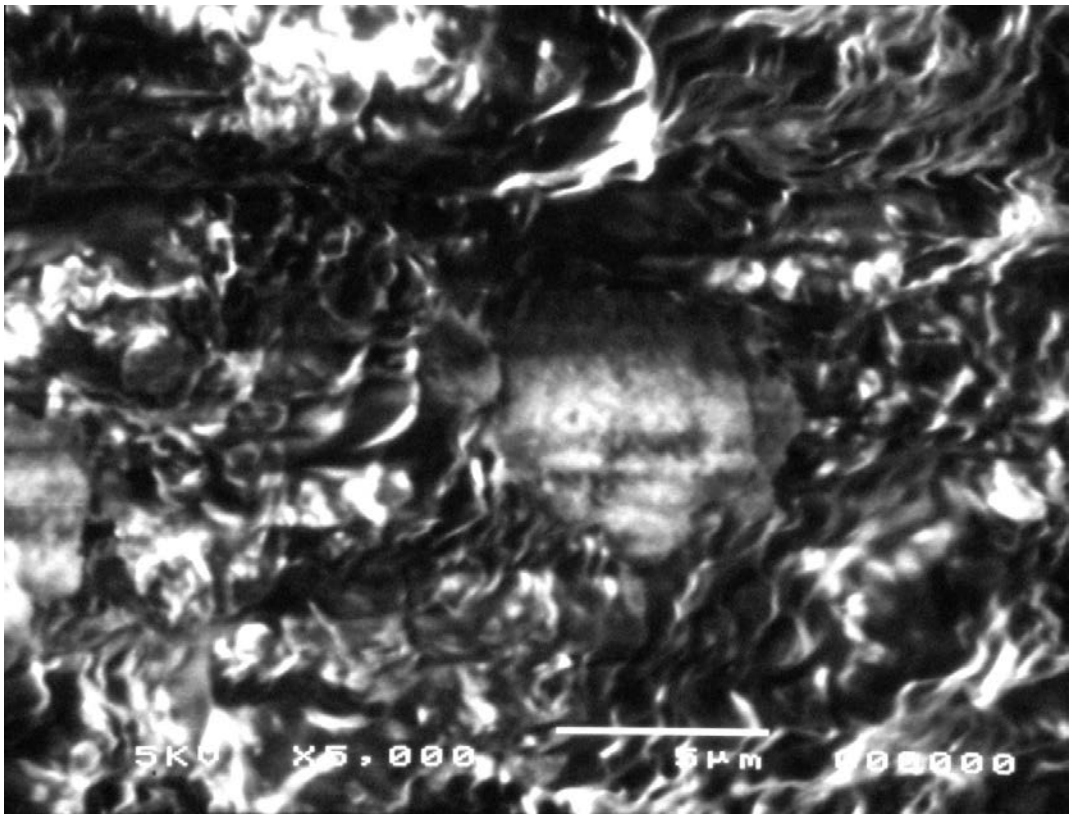

Fig. 14b. The same sample. Magnification 5000x, accelerating voltage 5 kV (another ROI)

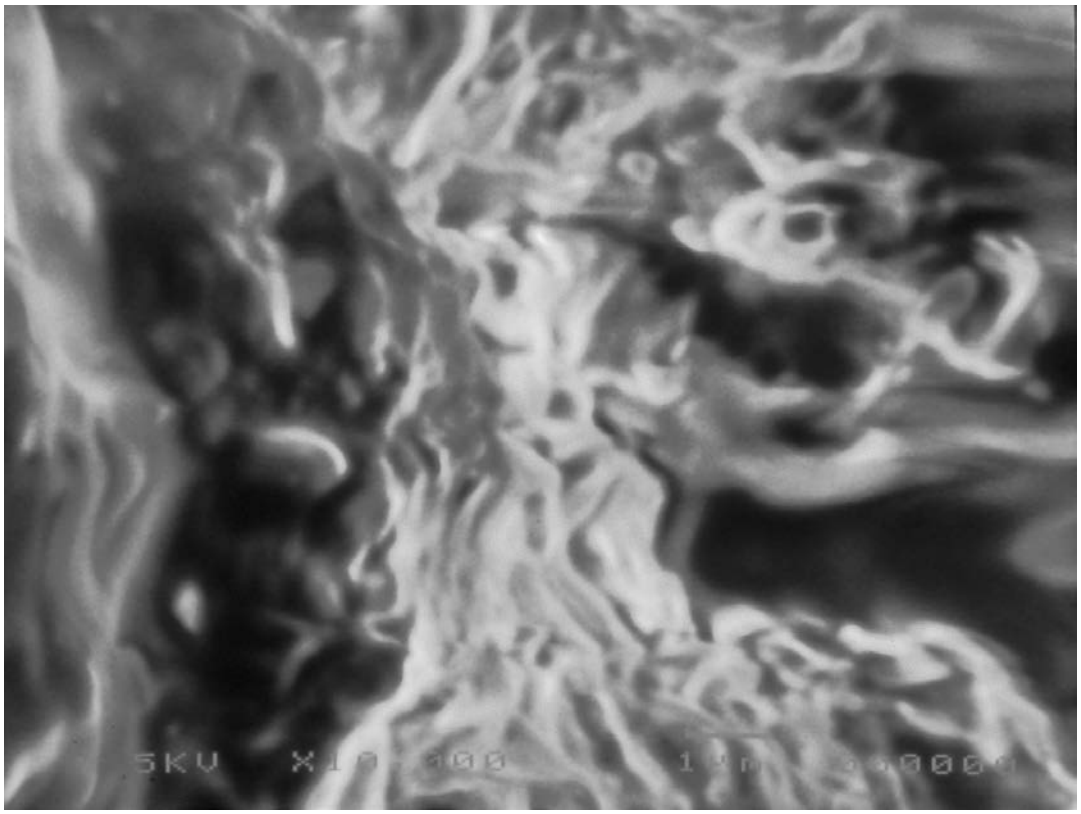

Fig. 15. The same sample. Magnification 10,000x, accelerating voltage 5 kV

4. Conclusion

Fossil elasmobranch teeth collected from multiple geographic regions, contrasting depositional settings, and different palaeo-oceans/palaeoclimates offer valuable archives of past marine conditions, but they pose a general analytical challenge for us: ensuring comparability among samples affected by locality-specific diagenesis. Primary biological and environmental signatures in enameloid and dentine can be partially overprinted by recrystallisation, mineral replacement, and post-burial elemental uptake. To discriminate these signals reliably, an integrated microstructural–geochemical workflow is required in which scanning electron microscopy is combined with electron-probe microanalysis with energy-dispersive (EDS) and wavelength-dispersive (WDS) X-ray spectroscopy. Deposits formed in different basins, palaeo-continents and palaeo-oceans commonly experienced contrasting diagenetic histories (chemistry, burial temperature, sedimentation time and substitution, redox state of the environment). These factors can overprint tooth tissues in ways that mimic or obscure primary biological/environmental signals. SEM provides the necessary taphonomic and microstructural context prior to geochemical interpretation. Backscattered-electron imaging and high-resolution secondary-electron imaging allow direct assessment of sample preservation states. SEM also resolves diagnostic enameloid ultrastructure, enabling the distinction between preserved biogenic fabrics and diagenetic mosaics that may mimic original biogenic features.

5. Author's contribution

1. Pavel L. Alexandrov – Automation of the electron microscope. Fabrication of an adapter for a camera. Designing and soldering circuits and connecting cables. Collection of elasmobranch teeth. Production of microphotographs of fossil teeth of elasmobranchs in the magnification range from 35 x to 10 000 x. Writing the "Materials and Methods" section and user manuals for users of the electron microscope digitized and upgraded by him.

2. Mikhail K. Filippov – Restorations of the vacuum systems, cleaning of the electron microscope column, commissioning of a new power supply source, replacement of technical oils.

3. Theodor K. Orekhov – Digital image processing using artificial intelligence. Writing a review on the applications of spectral methods and microprobe analysis (also using artificial intelligence and interactively). Working with open access spectral databases for mineral identification in fossil diagenesis and biomineralization processes.

6. Acknowledgements

The authors express their gratitude to the organizers of the Electron Microscopy Center of the Institute of Chemical Physics and the Institute of Energy Problems of Chemical Physics (2018–2019) for support of the research and to the participants of the joint project on biomedical engineering for funding the upgrade and restoration of the first electron microscope.

Statement on the Use of Artificial Intelligence

Artificial intelligence (AI) was used for this short technical note in English to refine the arguments supporting the feasibility of implementing electron microscopy, microprobe analysis, and X-ray spectroscopy methods by the last author (in 2025–2026).

Declaration of Absence of Conflict of Interest

The authors declare no conflict of interest between them.

References

Adnet et al., 1990 – *Adnet, S., Marivaux, L., Cappetta, H., Charruault, A.L., El Mabrouk, E., Jiquel, S., Ammar, H.K., Marandat, B., Marzougui, W., Merzeraud, G., Temani, R.* (2020). Diversity and renewal of tropical elasmobranchs around the Middle Eocene Climatic Optimum (MECO) in North Africa: New data from the lagoonal deposits of Djebel el Kébar, Central Tunisia. *Palaeontologia Electronica*. 23(2): a38.

Beavan, Russell, 1999 – *Beavan, N.R., Russell, A.P.* (1999). An elasmobranch assemblage from the terrestrial-marine transitional lethbridge coal zone (Dinosaur Park Formation: Upper Campanian), Alberta, Canada. *Journal of Paleontology*. 73(3): 494-503.

Boulemia, Adnet, 2023 – *Boulemia, S., Adnet, S.* (2023). A new Palaeogene elasmobranch fauna (Tebessa region, eastern Algeria) and the importance of Algerian-Tunisian phosphates for the North African fossil record. *Annales de Paléontologie*. 109(3): 102632.

Cappetta et al., 2006 – *Cappetta, H., Buffetaut, E., Cuny, G., Suteethorn, V.* (2006). A new elasmobranch assemblage from the Lower Cretaceous of Thailand. *Palaeontology*. 49(3): 547-555.

Daymond, 1999 – *Daymond, S.M.* (1999). Gondwanodus irwinensis gen. et sp. nov., a new elasmobranch from the Early Permian (Late Sakmarian) Fossil Cliff Member of the Holmwood Shale, Perth Basin, Western Australia. *Records – Western Australian Museum*. 19(4): 371-378.

Feichtinger et al., 2025 – *Feichtinger, I., Weinmann, A.E., Harzhauser, M., Schwarzhans, W., Golebiowski, R., Pollerspöck, J.* (2025). Deep-marine elasmobranchs from the Badenian (Langhian, Middle Miocene) of the Central Paratethys of Austria. *Austrian Journal of Earth Sciences*. 118(1): 205-217.

Höltke et al., 2023 – *Höltke, O., Salvador, R.B., Rasser, M.W.* (2023). Trophic relationships in the Early Miocene Upper Marine Molasse of Baden-Württemberg, Southwest Germany, with special emphasis on the elasmobranch fauna. *Palaeontologia Electronica*. 26(3): 1-38.

Iserbyt, De Schutter, 2012 – *Iserbyt, A., De Schutter, P.J.* (2012). Quantitative analysis of Elasmobranch assemblages from two successive Ypresian (early Eocene) facies at Marke, western Belgium. *Geologica belgica*. 15(3): 146-155.

Johns et al., 2014 – *Johns, M.J., Albanesi, G.L., Voldman, G.G.* (2014). Freshwater shark teeth (Family Lonchidiidae) from the Middle-Upper Triassic (Ladinian-Carnian) Paramillo Formation in the Mendoza Precordillera, Argentina. *Journal of Vertebrate Paleontology*. 34(3): 512-523.

Kocsis, 2024 – *Kocsis, L.* (2024). The elasmobranch fossil record of the Indo-Australian Archipelago since the Miocene: a literature review and new discoveries from Northern Borneo. *Diversity*. 16(6): 323.

Landini et al., 2017 – *Landini, W., Collareta, A., Pesci, F., Di Celma, C., Urbina, M., Bianucci, G.* (2017). A secondary nursery area for the copper shark Carcharhinus brachyurus from the late Miocene of Peru. *Journal of South American Earth Sciences*. 78: 164-174.

Leidner, Thies, 1999 – *Leidner, A., Thies, D.* (1999). Placoid scales and oral teeth of Late Jurassic elasmobranchs from Europe. *Mesozoic fishes*. 2: 29-40.

Lin et al., 2022 – *Lin, C.Y., Lin, C.H., Shimada, K.* (2022). A previously overlooked, highly diverse early Pleistocene elasmobranch assemblage from southern Taiwan. *PeerJ*. 10: e14190.

Long, 1992 – *Long, D.J.* (1992). Sharks from the La Meseta Formation (Eocene), Seymour Island, Antarctic Peninsula. *Journal of Vertebrate Paleontology*. 12(1): 11-32.

Mertiniene, 1995 – *Mertiniene, R.* (1995). The teeth of Symmorium reniforme cope from the Upper Carboniferous of the Moscow area (Russia). *Geobios*. 28: 147-150.

Mutter et al, 2007 – *Mutter, R.J., De Blanger, K., Neuman, A.G.* (2007). Elasmobranchs from the Lower Triassic Sulphur Mountain Formation near Wapiti Lake (BC, Canada). *Zoological Journal of the Linnean Society*. 149(3): 309-337.

Paton, 1993 – *Paton, R.L.* (1993). Elasmobranch fishes from the Viséan of East Kirkton, West Lothian, Scotland. *Earth and Environmental Science Transactions of The Royal Society of Edinburgh*. 84(3-4): 329-330.

Prasad et al., 2004 – *Prasad, G.V., Manhas, B. K., Arratia, G.* (2004). Elasmobranch and actinopterygian remains from the Jurassic and Cretaceous of India. *Mesozoic fishes*. 3: 625-638.

Prasad et al., 2017 – *Prasad, G.V., Verma, V., Sahni, A., Lourembam, R.S., Rajkumari, P.* (2017). Elasmobranch fauna from the upper most part of the Cretaceous Bagh Group, Narmada valley, India. *Island Arc*. 26(5): e12200.

Radwański, Marcinowski, 1996 – *Radwański, A., Marcinowski, R.* (1996). Elasmobranch teeth from the mid-Cretaceous sequence of the Mangyshlak Mountains, Western Kazakhstan. *Acta Geologica Polonica*. 46(1-2): 165-169.

Rees et al., 2024 – *Rees, J., Campbell, H.J., Simes, J.E.* (2024). The first Triassic elasmobranch teeth from the Southern Hemisphere (Canterbury, New Zealand). *New Zealand Journal of Geology and Geophysics*. 67(4): 426-433.

Schubert, 2013 – *Schubert, J.* (2013). Elasmobranch and osteichthyan fauna of the Rattlesnake Mountain Sandstone, Aguja Formation (Upper Cretaceous; Campanian), West Texas (Doctoral dissertation).

Schultz, 1977 – *Schultz, O.* (1977). Elasmobranch and teleost fish remains from the Korytnfca Clays (Middle Miocene; Holy Cross Mountains, Poland). *Acta Geologica Polonica*. 27(2): 201-210.

Shimada et al., 2015 – *Shimada, K., Popov, E.V., Siversson, M., Welton, B.J., Long, D.J.* (2015). A new clade of putative plankton-feeding sharks from the Upper Cretaceous of Russia and the United States. *Journal of Vertebrate Paleontology*. 35(5): e981335.

Smale, 2005 – *Smale, M.J.* (2005). The diet of the ragged-tooth shark Carcharias taurus Rafinesque 1810 in the Eastern Cape, South Africa. *African Journal of Marine Science*. 27(1): 331-335.

Sokolskyi, Guinot, 2021 – *Sokolskyi, T., Guinot, G.* (2021). Elasmobranch (chondrichthyes) assemblages from the Albian (lower Cretaceous) of Ukraine. *Cretaceous Research*. 117: 104603.

Suaez et al., 2004 – *Suarez, M., Encinas, A., Ward, D.* (2004). An Early Miocene elasmobranch fauna from the Navidad Formation, Central Chile, South America. *Cainozoic Research*. 4(1/2): 3-18.

Swinehart et al., 2020 – *Swinehart, A.L., Hoenig, M.M., Ginter, M.* (2020). A new addition to the Devonian elasmobranch fauna of Michigan, USA. *The American midland naturalist*. 184(1): 109-115.

Yun, 2021 – *Yun, C.G.* (2021). First deep-sea shark fossil teeth from the Miocene of South Korea. *Zoodiversity*. 55(3): 225-232.